Transport in Porous Media manuscript No.
(will be inserted by the editor)

Sensitivity Analysis and Quantification of the Role of Governing Transport Mechanisms and Parameters in a Gas Flow Model for Low Permeability Porous Media

Leonardo Sandoval · Monica Riva · Ivo Colombo · Alberto Guadagnini

Received: date / Accepted: date

Abstract Recent models represent gas (methane) migration in low permeability media as a weighted sum of various contributions, each associated with a given flow regime. These models typically embed numerous chemical/physical parameters that cannot be easily and unambiguously evaluated via experimental investigations. In this context, modern sensitivity analysis techniques enable us to diagnose the behavior of a given model through the quantification of the importance and role of model input uncertainties with respect to a target model output. Here, we rely on two global sensitivity analysis approaches and metrics (i.e., variance-based Sobol' indices and moment-based AMA indices) to assess the behavior of a recent interpretive model that conceptualizes gas migration as the sum of a surface diffusion mechanism and two weighted bulk flow components. We quantitatively investigate the impact of (i) each uncertain model parameter and (ii) the type of their associated probability distribution on the evaluation of methane flow. We then derive the structure of an effective diffusion coefficient embedding all complex mechanisms of the model considered and allowing quantification of the relative contribution of each flow mechanism to the overall gas flow.

Article Highlights

- Relative importance of parameters driving gas flow in low permeability media is assessed.
- The Influence of parameter probability distribution on gas flow statistics is appraised.
- A simple effective diffusion model embedding major methane flow mechanisms is derived.

L. Sandoval* (0000-0001-6264-9452) · M. Riva (0000-0002-7304-4114) · A. Guadagnini (0000-0003-3959-9690)
Dipartimento di Ingegneria Civile e Ambientale, Politecnico di Milano, Piazza L. da Vinci 32, 20133 Milano, Italy
* Corresponding author E-mail: rafaelleonardo.sandoval@polimi.it

I. Colombo (0000-0002-2888-6451)
Geolog Technologies, Via Monte Nero 30, 20098 San Giuliano Milanese, Italy

Keywords Gas flow · Nanopores · Bulk flow · Methane · Sensitivity Analysis

1 Introduction

Methane is recognized as a potential energy source to assist transition to a carbon free energy landscape (Hughes, 2013), considerable reserves of methane being associated with subsurface reservoirs worldwide (U.S. Energy Information Administration, 2015). After its generation, this gas typically accumulates in reservoir regions subdued to low permeability layers (i.e., caprocks) that prevent its upward migration (Dembicki-Jr., 2017). Due to the partial sealing efficiency of caprocks, some amount of gaseous phase hydrocarbons might cross such barrier and reservoir gas can then be released into the overburden to (eventually) reach the surface (Schlömer and Krooss, 1997; Schloemer and Krooss, 2004). In this context, appropriate modeling approaches to quantify gas migration in low-permeability geomaterials can assist the appraisal of the feasibility of a methane recovery project.

A variety of models depicting gas movement in low permeability geomaterials have been proposed (Wu et al., 2016; Sun et al., 2017; Rani et al., 2018; Wang et al., 2019). These models typically estimate the mass flow rate of gas as the result of a combination of various gas transport mechanisms taking place across the porous system. Parameters associated with these models, describing chemical, mechanical, flow, and transport features governing feedbacks between gas and the host rock matrix are always affected by uncertainty. The conceptual model of Wu et al. (2016) depicts the mass flow rate of a gas across a low permeability medium as the sum of three key processes: (i) a surface diffusion, and two weighted bulk diffusion components corresponding to (ii) slip flow and (iii) Knudsen diffusion. This model takes into account changes in the porous system caused by mechanical deformation and adsorption/desorption dynamics. The model embeds numerous parameters which are typically estimated through (direct or indirect) laboratory-scale experiments. Considering the set of complex mechanisms involved, these types of experiments are costly, time demanding, and their results are prone to uncertainty. The latter is also related to the intrinsic difficulties linked to replicating operational field conditions at the laboratory scale as well as to the challenges stemming from transferability of results to heterogeneous field scale settings (Pan et al., 2010; Yuan et al., 2014; Tan et al., 2018).

Due to our still incomplete knowledge of the critical mechanisms driving gas movement in low permeability media (Singh and Myong, 2018; Javadpour et al., 2021) and the complexities associated with the estimation of model parameters, model outputs should be carefully analyzed considering all possible (aleatoric and epistemic) sources of uncertainty. In this sense, sensitivity analysis approaches are important tools enabling us to (i) quantify uncertainty, (ii) enhance our understanding of the relationships between model inputs and outputs, and (iii) tackle the challenges of model- and data-driven design of experiments (Dell'Oca et al., 2017). Hence, sensitivity analysis techniques may be effectively used in the context of methane flow modeling efforts to (i) quantify and rank the contribution of our lack of knowledge on each model parameter to the uncertainty associated with model outputs; (ii) identify model input-output relationships; and (iii) enhance the quality of parameter estimation workflows, upon focusing efforts on parameters with the highest influence to target model outputs (Saltelli et al., 2010;

Dell'Oca et al., 2020). In cases where parameters associated with a model have already been estimated (e.g., through model calibration), the main purpose of a Global Sensitivity Analysis, GSA, is to quantify the uncertainty still remaining after model calibration, thus guiding additional efforts for its characterization (e.g., Dell'Oca et al. (2020) and references therein). The probability density function (pdf) associated with each model parameter at this stage will possibly be different from the one employed before model calibration and some model parameters might be associated with a reduced uncertainty. In cases where processes are described through black-box models, GSA can be employed to quantify the influence that the variability of hyperparameters embedded in these models can have on their outcomes. We note that if uncertainty of some model parameters is further constrained, for example through stochastic inverse modeling (e.g., Ceresa et al. (2021)), results of the uncertainty quantification might also change. In this work we illustrate the methodological framework and the workflow required for GSA of a methane flow model and provide the elements to perform such an analysis for diverse scenarios. In order to assist this process, we provide a repository with scripts developed during this work (see declaration section).

In this work we rely on GSA approaches to study the behavior of the aforementioned gas migration model targeting low permeability media. While previous works focus on only a few selected model parameters (Song et al., 2016; Wu et al., 2017; Sun et al., 2017), a comprehensive diagnosis of the system behavior based on rigorous and modern GSA approaches taking into account the way all model parameters influence model output uncertainty is still missing. Here, we do so by implementing two GSA techniques, respectively based on the evaluation of (i) the classical (variance-based) Sobol' indices (Saltelli and Sobol', 1995) and (ii) the recent moment-based GSA metrics proposed by Dell'Oca et al. (2017). We recall that GSA approaches relying on Sobol' indices are widely used to quantify the relative expected reduction of variance of the target model output due to the knowledge of (or conditioning on) a given parameter. These have been employed in several applications, including diagnosis of models related to, e.g., flood risk assessment (Koks et al., 2015), overpressure risk assessment in sedimentary basins (Colombo et al., 2017), and energy storage (Xiao et al., 2021). A critical limitation of variance-based GSA methodologies is that the uncertainty of the output is considered to be completely characterized by its variance. Such an assumption can lead to an incomplete characterization of the system behavior. The moment-based GSA approach introduced by Dell'Oca et al. (2017) is designed to enhance our capability to evidence model behavior upon including the quantification of model parameter uncertainty on the (statistical) moments of the pdf of a model output of interest. As such, this comprehensive approach yields information enabling us to characterize various aspects of uncertainty, without being limited solely to the concept of variance. The ensuing indices (termed AMA indices, after the initials of the authors (Dell'Oca et al., 2017)) have been effectively employed in a variety of contexts, including geophysical analyses related to gravimetric responses due to pumping tests (Maina et al., 2021), biochemical degradation of compounds such as gliphosate in soils (la Cecilia et al., 2020), and groundwater flow, including its feedbacks with evapotranspiration (Bianchi Janetti et al., 2019; Maina and Siirila-Woodburn, 2020).

This work is organized as follows: Section 2.1 briefly illustrates the complete model we consider to describe methane flow in low permeability media. The main theoretical elements of the GSA approaches employed are described in Section 2.2. Key results of the GSA are presented in Section 3. Here, we also derive and discuss novel effective diffusive formulations, which have the ability to encapsulate all physical-chemical mechanism included in the full methane flow model described in Section 2.1. Finally, conclusions are drawn in Section 4.

2 Materials and Methods

2.1 Gas flow in low permeability media

Models adopted to quantify gas migration in low permeability media can be classified according to their complexity, in terms of, e.g., conceptualization and mathematical rendering of the embedded processes, as well as number of their characteristic parameters. Among existing models associated with a high degree of complexity and including multiple transport processes jointly contributing to the total gas migration across the system (Mehmani et al., 2013; Wu et al., 2015a, 2016, 2017; Sun et al., 2017; Zhang et al., 2018; Javadpour et al., 2021), here we consider the model of Wu et al. (2016). The selected model allows considering mechanical deformation as well as relevant features associated with real gases such as variations in the gas viscosity (η), and the effects of the compressibility (C_g) and gas deviation (Z) factors caused by pressure and temperature changes.

The model introduced by Wu et al. (2016) rests on a conceptual picture according to which the total mass flow rate of gas per unit of area (J) is rendered through the sum of (i) a surface diffusion (J_s) and two weighted bulk diffusion components, corresponding to (ii) slip flow (J_v), and (iii) Knudsen diffusion (J_k), i.e.,

$$J = J_s + w_v J_v + w_k J_k. \tag{1}$$

The surface diffusion component is given by (Wu et al., 2015b)

$$J_s = -\zeta_{ms} \frac{D_s C_{sc}}{p} \frac{\partial p}{\partial l}, \tag{2}$$

where p is (gas) pore pressure and $\frac{\partial p}{\partial l}$ represents the strength of the driving force through the system, corresponding to the spatial gradient of gas pore pressure. The (dimensionless) coefficient ζ_{ms} is intended to take into account the possibility of applying the model (originally developed for capillary tubes) to a complex pore space and is defined in Equation (17) of the Appendix where it is shown that ζ_{ms} depends on porosity (ϕ), tortuosity (τ), pore size (r) (i.e. pore radius), and gas coverage on the geomaterial (θ). The term D_s in Equation (2) is the surface diffusion coefficient, which is expressed (as shown in Equation (25)) in terms of gas temperature (T), isosteric adsorption heat of the geomaterial (ΔH), a parameter (κ) related to the blockage/migration ratio of the adsorbed molecules, and θ. Finally, C_{sc}, defined in Equation (28), is the adsorbed concentration, which in turn depends on θ and on the gas molecule diameter (d_m).

The model proposed by Wu et al. (2016) allows representing the mechanical deformation of the pore space (in terms of variation of permeability and porosity with pressure) through power-law relationships and making use of the classical Kozeny-Carman equation. Here, we rest on their original model formulation, which naturally leads to Equations (19) and (20), clearly evidencing that both r and ϕ evolve with p as a function of a reference pore radius (r_o) and reference porosity (ϕ_o), respectively.

The weight coefficients of the slip flow (w_v) and Knudsen diffusion (w_k) components in Equation (1) are given by (Wu et al., 2016)

$$w_v = \frac{1}{1+K_n}, \tag{3}$$

$$w_k = \frac{1}{1+1/K_n}. \tag{4}$$

Here, K_n is the (dimensionless) Knudsen number defined as

$$K_n = \frac{\lambda}{2r}, \tag{5}$$

with

$$\lambda = \frac{\eta}{p}\sqrt{\frac{\pi ZRT}{2M}}, \tag{6}$$

where M and R are the gas molar mass and universal constant, respectively. Note that K_n relates the mean free path of the gas molecules (λ) to a representative length of the system (Civan, 2010), here taken as the pore diameter.

The slip flow component is dominant in systems where $K_n < 0.1$ (Ziarani and Aguilera, 2012) and can be evaluated as (Karniadakis et al., 2005; Wu et al., 2016)

$$J_v = -\zeta_{mb}\frac{r^2 pM}{8\eta ZRT}(1+\alpha K_n)\left(1+\frac{4K_n}{1+K_n}\right)\frac{\partial p}{\partial l}. \tag{7}$$

Here, ζ_{mb} is intended to take into account the possibility of applying the slip flow formulation (7) to a complex pore space (see Eq. (23)) and α is the rarified effect coefficient for a real gas which, according to Karniadakis et al. (2005), is evaluated through Equation (24).

The Knudsen flow component is dominant in systems where $K_n > 10$ (Ziarani and Aguilera, 2012) and is evaluated as (Darabi et al., 2012; Liu et al., 2016)

$$J_k = -\frac{2}{3}\zeta_{mb} r\delta^{D_f-2}\left(\frac{8ZM}{\pi RT}\right)^{1/2}\frac{p}{Z}C_g\frac{\partial p}{\partial l}. \tag{8}$$

Here, D_f represents the fractal dimension of the pore surface and δ denotes the ratio between d_m and r.

We conclude by noting that the model here described includes a total of 15 parameters, which are related to the richness of physical processes embedded therein (See also Section 3.3). All quantities here introduced are listed in Table 1 and in the list of symbols and nomenclature Section.

2.2 Global Sensitivity Analysis

We perform a rigorous sensitivity analysis of the model illustrated in Section 2.1 to diagnose its behavior with reference to the estimate of methane flow as driven by imperfect knowledge of the associated parameters. Here, the uncertainty associated with the selection of the interpretative model is not analyzed. Nevertheless, one could also consider quantification of uncertainty of model outputs in the presence of uncertain interpretive models. In this context, uncertainty of a target variable which might result from the use of a collection of interpretive (conceptual and mathematical) models, could be assessed upon relying, for example, on the approach illustrated by Dell'Oca et al. (2020). Our analysis is intended to yield a robust quantification of the relative importance of uncertain model parameters to a model output of interest. As mentioned in the Introduction, we rely on two GSA approaches, corresponding to (i) the classical variance-based technique grounded on the evaluation of the well-known Sobol' indices (Saltelli and Sobol', 1995) and (ii) the moment-based GSA framework introduced by Dell'Oca et al. (2017).

Model parameters are treated as statistically independent, as the amount of available information does not enable us to clearly identify cross-correlations amongst parameters and to quantify joint distributions. We consider three differing characterizations of pdf describing uncertainty of model parameters: (a) all parameters are represented through uniform pdfs, (b) all parameters are represented by truncated Gaussian pdfs, and (c) the reference pore radius is characterized by a (truncated) log-normal pdf, while all remaining parameters are associated with uniform pdfs. Case a is representative of an approach where information on the considered parameters is limited so that all parameter values within the identified range of variability are equally weighted in the analysis (other studies relying on the same assumption include, e.g., Ciriello et al. (2013); Laloy et al. (2013); Sochala and Le Maître (2013); Bianchi Janetti et al. (2019); Dell'Oca et al. (2020)). Case b is implemented as an alternative uninformed case, making use of the widely adopted hypothesis that model parameters are normally distributed. Case c takes advantage of the findings of Naraghi et al. (2018) who provide some experimental evidence suggesting that the pdf of pore radii in shales can be interpreted through a log-normal model. Our choice of performing sensitivity analyses according to configurations associated with diverse pdfs characterizing uncertain model parameters enables us to analyze the influence of model parameter pdf (which is generally unknown a priori) on the results of the GSA and, ultimately, on gas flow forecasting.

Considering the computational cost associated with multiple model evaluations (corresponding to 10^{-4} seconds per simulation on an Intel Xeon Gold 6148 CPU @ 2.4 GHz) required for these analyses and the corresponding cost for random sampling across the considered high dimensionality model parameter space, our analyses rest on 10^8 model evaluations. The latter has been deemed to constitute an acceptable trade-off between the need to obtain stable results and computational efforts (details not shown). The pressure gradient acting on the system is set as a given boundary condition (and equal to 0.1MPa/m) in all test cases.

2.2.1 Variance-based Sobol' Indices

Sobol' indices (Saltelli and Sobol', 1995) can assist the appraisal and quantification of the relative expected reduction of the variance of a target model output due to knowledge of (or conditioning on) a given model parameter, which would otherwise be subject to uncertainty. In this context, considering a model output y, which depends on N random parameters collected in vector $\mathbf{x} = (x_1, x_2, ..., x_N)$ and defined within the space $\Gamma = \Gamma_1 \times \Gamma_2 \times ... \times \Gamma_N$ ($\Gamma_i = [x_{i,min}, x_{i,max}]$ corresponding to the support of the i-th parameter, x_i), the principal Sobol' index S_{x_i} associated with a given model parameter x_i is evaluated as

$$S_{x_i} = \frac{V\left[E\left[y|x_i\right]\right]}{V\left[y\right]}. \tag{9}$$

Here, $E\left[\cdot\right]$ and $V\left[\cdot\right]$ represent expectation and variance operators, respectively; the notation $y|x_i$ denotes conditioning of y on x_i. Note that S_{x_i} describes the relative contribution to $V[y]$ due to variability of only x_i. Joint contributions of x_i with other model parameters included in $\mathbf{x}$ to the variance of y are embedded in the total Sobol' indices (details not shown). We recall that relying on Sobol' indices to diagnose the relative importance of uncertain model parameters to model outputs is tantamount to identifying uncertainty with the concept of variance of a pdf. As such, while Sobol' indices are characterized by a conceptual simplicity and straightforward implementation and use, they provide only limited information about the way variations of model parameters can influence the complete pdf of model outputs.

2.2.2 Moment-Based AMA Indices

The recent moment-based GSA approach proposed by Dell'Oca et al. (2017, 2020) rests on the idea that the quantification of the effects of model parameter uncertainty on various statistical moments of the ensuing pdf of model outputs can provide enhanced understanding of model functioning. Dell'Oca et al. (2017) introduce Moment-Based sensitivity metrics (termed AMA indices) according to which one can evaluate the influence of uncertain model parameter on key elements of the model output pdf, as embedded in its associated statistical moments. The AMA indices are defined as follows (Dell'Oca et al. (2017)):

$$\mathrm{AMA}M_{x_i} = \frac{1}{|M[y]|} E\left[|M[y] - M\left[y|x_i\right]|\right]. \tag{10}$$

Here, $\mathrm{AMA}M_{x_i}$ represents the indices associated with a model parameter x_i and a given statistical moment M of the pdf of model output y (considering the first four statistical moments of y, $M = E$ for the mean, $M = V$ for the variance, $M = \gamma$ for the skewness, and $M = k$ for the kurtosis). The AMA indices are intended to quantify the expected change of each statistical moment of y due to our knowledge of x_i. Large values of these indices indicate that variations of the associated parameter strongly affect the statistical moments of y.

Table 1 Ranges of variability for the methane migration model uncertain parameters considered in the GSA. Coefficient of variation, criteria for the selection of the range of variability, and reference considered for the definition of each range of variability is also listed.

Parameter - (Units) - Symbol	Range (CV%)	Criteria support	Reference
Reference pore radius - (nm) - r_o	2-100 (55)	Literature	Wu et al. (2016)
Reference porosity - (-) - ϕ_o	0.005-0.1 (52)	Literature	Li et al. (2006)
Pore pressure - (MPa) - p	0.5-50 (57)	Literature	Wu et al. (2016)
Tortuosity - (-) - τ	2.8-5.8 (20)	Literature	Mohd Amin et al. (2014)
Temperature - (K) - T	337-473 (10)	Literature	Chiquet et al. (2007)
Overburden pressure - (MPa) - p_c	51-90 (16)	Literature	Chiquet et al. (2007)
Porosity exponent - (-) - q	0.014-0.056 (35)	Literature	Dong et al. (2010)
Pore radius exponent - (-) - t	0.02-0.04 (19)	Literature	Dong et al. (2010)
Block/migration ratio - (-) - κ	0.1-2 (52)	Literature	Wu et al. (2015b)
Fractal dimension - (-) - D_f	2.1-2.9 (9)	Theoretical Limits	Coppens (1999)
Isosteric adsorption heat - (J/mol) - ΔH	12000-16000 (8)	Literature	Wu et al. (2015b)
Reference Langmuir pressure - (Pa) - p_{L_o}	41-128 (30)	CV	Wu et al. (2015b)
Parameter - (-) - α_0	1.02-1.36 (8)	Literature	Karniadakis et al. (2005)
Parameter - (-) - α_1	2-6 (30)	CV	Karniadakis et al. (2005)
Parameter - (-) - β	0.2-0.6 (30)	CV	Karniadakis et al. (2005)

3 Results and Discussion

3.1 GSA of methane flow model

The 15 uncertain model parameters of model (1) are considered to vary across the support defined through the ranges of variability listed in Table 1. These ranges have been designed upon considering available literature references (values typically employed for the model parameters in low permeability geomaterials). With reference to three of the model parameters, i.e., L_{p_o}, α_1 and β, only very limited information is available from the literature, to the best of our knowledge (Karniadakis et al., 2005). Thus, we take the values considered by Wu et al. (2017) and Karniadakis et al. (2005) as the centers of corresponding intervals of variability associated with a given coefficient of variation, that we set equal to 30%, which enables us to imprint these parameters with a sufficiently broad range of variability, similar to what found for the remaining uncertain parameters (see Table 1). Finally, we allow the fractal dimension D_f to vary within its theoretical bounds (i.e., 2< D_f <3) (Coppens, 1999; Coppens and Dammers, 2006). Methane properties (such as viscosity, compressibility, and deviation factor) are estimated using miniREFPROP (Lemmon et al., 2018), a tool that incorporates equations of state for a variety of gas species. With reference to methane miniREFPROP relies on the equation of state proposed by Setzmann and Wagner (1991).

Table 2 lists the moment-based GSA indices related to mean (AMAE_{x_i}), variance (AMAV_{x_i}), skewness (AMAγ_{x_i}), and kurtosis (AMAk_{x_i}) of J as well as the principal Sobol' indices (S_{x_i}) evaluated for methane flow rate values rendered by Eq. (1) for the case in which all model parameters are modeled as independent and identically distributed random variables, each characterized by a uniform pdf (Case a).

While the strength of the influence of the reference pore radius (r_o) on the model output is not the same for the (first four) statistical moments, the AMA indices clearly suggest that conditioning on r_o has (overall) the strongest impact on the first four statistical moments of methane flow. This is then followed by reference porosity, pore pressure, tortuosity, and temperature. While the remaining

Table 2 Moment-based GSA indices AMAM_{x_i} and Sobol' principal indices S_{x_i} for all x_i parameters included in Equation (1). All model parameters are described by uniform pdfs (Case a). Values of each metric identifying the most influential parameters are reported in bold.

x_i	AMAE_{x_i}	AMAV_{x_i}	S_{x_i}	AMAγ_{x_i}	AMAk_{x_i}
r_o	**0.728**	**0.798**	**0.417**	**0.562**	**0.757**
ϕ_o	**0.453**	**0.643**	**0.160**	**0.345**	**0.464**
p	**0.335**	**0.484**	**0.091**	**0.208**	**0.476**
τ	**0.181**	**0.356**	0.026	**0.114**	**0.213**
T	0.094	**0.163**	0.007	0.027	0.046
q	0.061	0.119	0.003	0.011	0.022
t	0.057	0.114	0.003	0.01	0.021
p_c	0.028	0.063	0.001	0.008	0.014
κ	0.010	0.005	0	0.004	0.007
ΔH	0.001	0.002	0	0.002	0.005
D_f	0.002	0.003	0	0.002	0.004
p_{L_o}	0.002	0.003	0	0.002	0.004
α_0	0.001	0.002	0	0.002	0.004
α_1	0.001	0.002	0	0.002	0.004
β	0.001	0.002	0	0.002	0.004

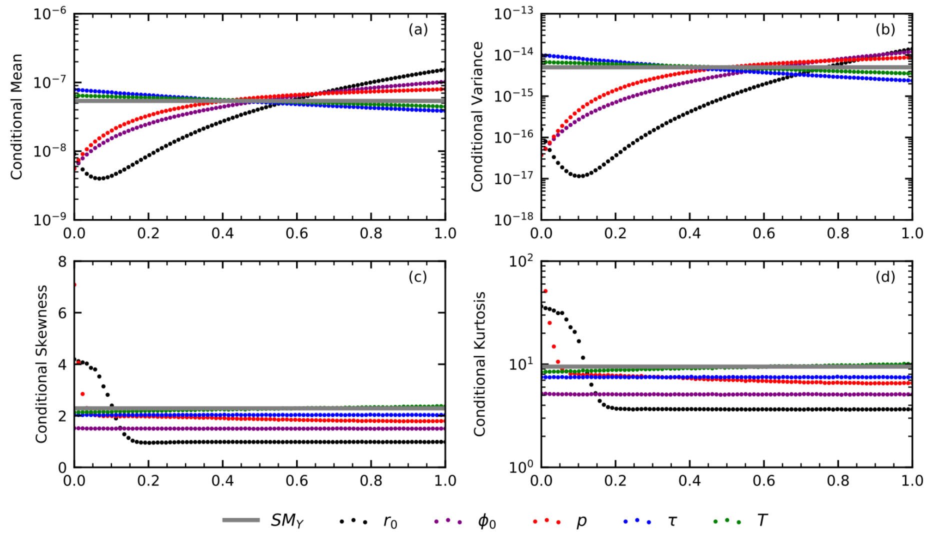

Fig. 1 First four statistical moments of methane flow J (Ton/m^2 year) conditional on values of the most influential model parameters (see Table 2): (a) expected value, (b) variance, (c) skewness, and (d) kurtosis. The corresponding unconditional moments (i.e. SM_Y) are also depicted (gray bold horizontal lines). Intervals of variation of the uncertain model parameters are rescaled within the unit interval for graphical representation purposes. All model parameters are described by uniform pdfs (Case a).

model uncertain parameters still exert some influence on the (first four) statistical moments of J (as evidenced by the non-zero values of AMA indices), the strength of their influence can be considered as marginal when compared to the above mentioned quantities, which are seen to be key in driving the main features of the pdf of methane flow. In the following we denote as *most influential parameters* for metrics AMAM_{x_i} or S_{x_i} all parameters x_i where AMA$M_{x_i}/\sum_{x_i}$ AMA$M_{x_i} \geq 5\%$ or $S_{x_i}/\sum_{x_i} S_{x_i} \geq 5\%$, respectively. Most influential parameters identified by each metric are reported in bold in Table 2. Values of the Sobol' principal indices are generally consistent with the results stemming from the moment-based GSA, even as τ and T are not identified as influential to the model output according to the Sobol' principal index. This result is consistent with the observation that conditional variance can be larger or smaller than its unconditional counterpart (see also Fig. 1b) in a way that its integral over Γ_T vanishes. A similar effect associated with the principal Sobol' indices was identified by Dell'Oca et al. (2017) with reference to the Ishigami function, which is a widely used analytical benchmark in sensitivity studies.

Figure 1 depicts the first four statistical moments of J conditioned on values of the five most influential uncertain parameters selected on the basis of Table 2. Uncertain parameters are normalized to span the unit interval, for ease of interpretation. Unconditional moments are also depicted as a reference. We note that when considering conditioning on the model parameters which have been identified as non-influential according to the metrics employed, the difference between conditional and unconditional moments is negligible (details not reported).

As expected, conditioning on values of the reference pore radius (r_o) yields the most marked effects to all of the statistical moments considered (see black dotted curves in Figure 1). Mean and variance of methane flow generally increase with r_o. A minimum mean methane flow value is attained for $2< r_o <15$ nm (corresponding to the range of normalized values comprised between 0 and 0.15 in Figure 1). The dominant transport mechanism for $r_o <15$ nm is surface diffusion, the strength of its contribution decreasing with increasing r_o. As r_o increases, the strength of the contribution related to surface diffusion decreases faster than the corresponding increase of the slip flow contribution, thus resulting in a minimum value for the expected methane flow for values of the reference pore radius comprised in the aforementioned range. Otherwise, skewness and kurtosis (i) are affected by variations of the reference pore radius when the latter is smaller than 20 nm (corresponding to a normalized value of 0.18); and (ii) are generally constant for $r_o >$ 20 nm. Nevertheless, we note that these (statistical) moments are still remarkably different from their unconditional counterparts even for large r_o values, thus evidencing the impact of acquired knowledge on r_o on reducing the asymmetry (as rendered by the skewness) and the peakedness and tailedness (i.e., the probability associated with extreme values, as rendered by the kurtosis) of the methane flow pdf.

Conditioning on pore pressure imprints variations to the statistics of the model output which are qualitatively similar to those associated with r_o. Larger values of mean and variance of J are linked to larger values of p. This result descends from the linear relationship between pore pressure and slip flow (Equation (7)), the latter being the dominant mechanism in systems formed by larger pores. Conditional skewness and kurtosis are constant (albeit different from their unconditional counterpart) across most of the variability range of p, sharp variations of these quantities being associated with conditioning on low values of p (i.e., corresponding to pore pressure values smaller than 10 MPa). Our findings about the influence of p on J are consistent with the results of Sun et al. (2017). These authors find that increasing values of pore pressure lead to an increase of apparent permeability (which is in turn linearly proportional to gas flow) for $r_o > 10$ nm. Wu et al. (2016) document a similar behavior due to the dominance of the slip flow component (which is proportional to p; see Equation (7)) in systems characterized by large pores.

While the impact of reference porosity and tortuosity is not analyzed in any of the available previous studies (Wu et al., 2015b, 2016, 2017; Sun et al., 2017; Zhang et al., 2018), our results rank ϕ_o and τ as the second and fourth most influential parameters in the evaluation of the pdf of J, respectively (see Table 2). The correction factors for bulk (eq. (23)) and surface (eq. (17)) diffusion flow increase linearly with reference porosity. Thus, increased values of ϕ_o yield corresponding increases of the methane flow (and hence of its first two statistical moments) independent of the dominant transport mechanism. Conditional mean and variance of J decrease with increasing values of tortuosity. This is in line with the observation that all gas transport mechanisms are characterized by an inverse proportionality between J and τ through the correction factor which is related to these processes taking place within a porous domain. These elements are consistent with a physical picture according to which fluid flow rates across a porous geomaterial are expected to increase and decrease with increasing porosity and tortuosity, respectively. Unlike pore pressure and reference pore radius, conditioning on reference porosity and tortuosity yields a reduction of skewness and kurtosis of the pdf of J, whose conditional values remain constant independent of the value of ϕ_o and/or τ.

Conditioning on temperature (T) affects the mean and variance of the methane flow pdf in a way which is qualitatively similar to the effect of tortuosity (albeit quantitatively to a lesser extent) due to the inverse proportionality between J and T. Otherwise, the overall shape of the pdf of J is not significantly influenced by the knowledge of T, values of conditional skewness and kurtosis practically coinciding with their unconditional counterparts.

The results listed in Table 2 suggest that statistical moments of methane flow are virtually insensitive to the remaining parameters (i.e., 10 of the 15 model parameters). Therefore, setting any of these parameters at given values within the variability space considered in our analysis yields only minor changes in the prediction of J. In this context, our results suggest that methane flow can be assessed with an acceptable degree of reliability even in the presence of scarce information about several parameters embedded in Equation (1) such as, e.g., the overburden pressure (i.e., p_c), the power-law exponents related to porosity (i.e., q) and pore radius (i.e., t), the fractal dimension of the pore surface (i.e.,D_f), or the isosteric adsorption heat of the geomaterial (i.e., ΔH). Further to this, our results suggest the opportunity to prioritize allocation of resources to robust characterization of (in descending order) reference pore radius, reference porosity, pore pressure, tortuosity, and temperature.

3.2 Impact of the model parameter pdfs on GSA results

In this section we analyze the impact of the choice of model parameter distribution on the pdf of J. As described in Section 2.2, we compare the GSA outcomes obtained with a uniform pdf for all model parameters (Case a) and illustrated in Section 3.1 against those computed when (i) all model parameters are characterized through (truncated) Gaussian pdfs (Case b) and (ii) r_o is described by a (truncated) log-normal pdf while the remaining parameters are described as in

Table 3 Moment-based GSA indices AMAM_{x_i} and Sobol' principal indices S_{x_i} for all x_i parameters included in Equation (1). All model parameters are described by truncated Gaussian distributions (Case b). Values of each metric identifying the most influential parameters are reported in bold.

x_i	AMAE_{x_i}	AMAV_{x_i}	S_{x_i}	AMAγ_{x_i}	AMAk_{x_i}
r_o	**0.787**	**0.828**	**0.761**	**0.608**	**0.692**
ϕ_o	**0.452**	**0.674**	**0.242**	**0.306**	**0.402**
p	**0.321**	**0.481**	**0.131**	**0.152**	**0.302**
τ	**0.182**	**0.363**	0.041	**0.088**	**0.157**
T	**0.100**	**0.178**	0.012	0.027	0.042
q	0.063	0.122	0.005	0.010	0.018
t	0.059	0.117	0.004	0.009	0.016
p_c	0.025	0.056	0.001	0.006	0.011
κ	0.007	0.005	0	0.005	0.008
ΔH	0.001	0.002	0	0.003	0.007
D_f	0.001	0.003	0	0.002	0.005
p_{L_o}	0.001	0.002	0	0.003	0.006
α_0	0.001	0.002	0	0.002	0.005
α_1	0.001	0.002	0	0.003	0.006
β	0.001	0.002	0	0.003	0.006

Case a (Case c). To provide a consistent comparison, Gaussian and log-normal pdfs are defined to honor the same mean and variance of the scenario associated with Case a.

Table 3 lists values of AMA and principal Sobol' indices for each of the parameters embedded in Equation (1) for Case b. Results of Table 3 and Table 2 are qualitatively similar, i.e., the GSA yields similar results considering a uniform or a (truncated) Gaussian pdf for all model parameters. Our results imbue us with confidence about the documented ranking of parameter importance, with reference pore radius, reference porosity, pore pressure, tortuosity, and temperature identified as the model parameters being the key drivers to the evaluation of the major features of the pdf of methane flow. Values of statistical moments of J conditioned on model parameters for Case b are very similar to those depicted in Figure 1 for Case a (details not shown).

Table 4 lists the AMA and the principal Sobol' indices associated with J for Case c. In this case, it is even more evident that the uncertainty of r_o is strongly dominant on the evaluation of the pdf of methane flow. Additionally, the blockage/migration ratio of the adsorbed molecules (κ) gains importance with respect to previous cases, quantitatively impacting the pdf of J to an extent which is similar to what exhibited by temperature. This feature is attributed to the abundance of small pores in this scenario, which favors the dominance of the surface diffusion flow mechanism (linked to parameter κ).

Figure 2 depicts the first four statistical moments of methane flow conditioned on values of influential uncertain parameters for Case c (see Table 4). Unconditional moments are also shown as a reference. Overall, the results are qualitatively similar to those embedded in Figure 1 for Case a. The unconditional mean and variance of J in Case c are reduced (to approximately one-fourth and one-sixth, respectively) with respect to the corresponding values for Case a. Otherwise, unconditional skewness and kurtosis increase by about 2.6 and 6 times, respectively.

Table 4 Moment-based GSA indices AMAM_{x_i} and Sobol' principal indices S_{x_i} for all x_i parameters included in Equation (1). Reference pore radius (r_o) is described by a (truncated) lognormal distribution and the remaining model parameters are described by uniform distributions (Case c). Values of each metric identifying the most influential parameters are reported in bold.

x_i	AMAE_{x_i}	AMAV_{x_i}	S_{x_i}	AMAγ_{x_i}	AMAk_{x_i}
r_o	**3.332**	**3.649**	**2.803**	**0.788**	**0.883**
ϕ_o	**0.452**	**0.690**	0.064	**0.212**	**0.404**
p	0.192	**0.507**	0.012	**0.152**	**0.263**
τ	0.181	**0.358**	0.011	**0.070**	**0.167**
T	0.090	0.173	0.003	0.024	0.050
q	0.063	0.121	0.001	0.008	0.020
t	0.041	0.112	0.001	0.008	0.020
p_c	0.023	0.061	0	0.007	0.016
κ	0.112	0.010	0.005	0.021	0.027
ΔH	0.002	0.006	0	0.004	0.010
D_f	0.02	0.008	0	0.011	0.018
p_{L_o}	0.025	0.007	0	0.011	0.017
α_0	0.002	0.006	0	0.005	0.013
α_1	0.002	0.006	0	0.005	0.012
β	0.002	0.006	0	0.004	0.010

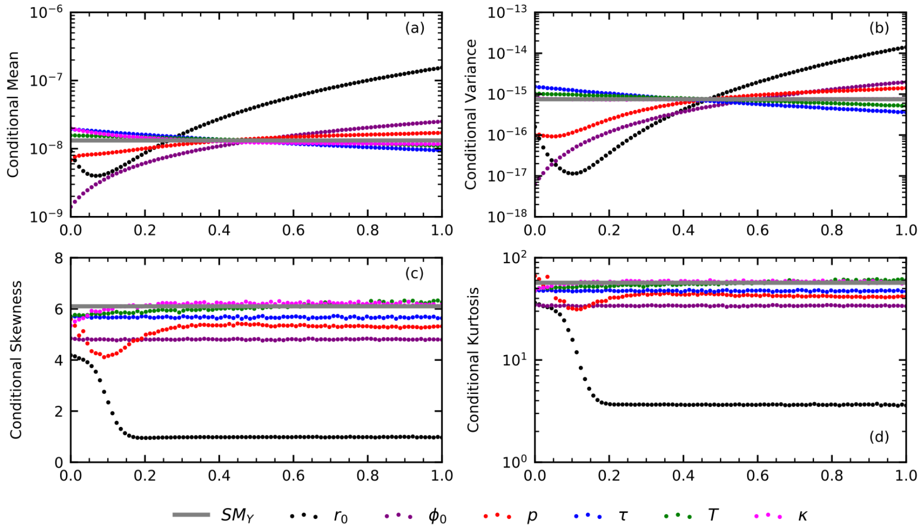

Fig. 2 First four statistical moments of methane flow J (Ton/m^2 year) conditional on values of the most influential model parameters (see Table 4): (a) expected value, (b) variance, (c) skewness, and (d) kurtosis. The corresponding unconditional moments (i.e. SM_Y) are also depicted (gray bold horizontal lines). Intervals of variation of the uncertain model parameters are rescaled within the unit interval for graphical representation purposes. r_o is described by a truncated log-normal pdf and the remaining model parameters are described by uniform pdfs (Case c).

These behaviors are attributed to the larger frequency of small reference pore radius values considered in Case c with respect to Case a (and b). Low values of reference pore radius are associated with large values of surface diffusion and to small values of mean and variance of methane flow. Conditioning on r_o and ϕ_o imprints variations to the model output mean and variance across the entire range of variability of these parameters (Figure 2). We further note that conditioning on r_o strongly reduces skewness and kurtosis of the pdf of J, thus reducing the probability associated with extreme (large) values of J.

Conditioning on p induces variations in the (first four) statistical moments of the model output. Conditioning on larger values of this quantity yields the highest values of mean and variance of the model output. A minimum in the values of conditional variance, skewness, and kurtosis is observed in the interval 1MPa< p <15MPa. Finally, the blockage/migration ratio of adsorbed molecules displays (a small but noticeable) influence on the model output pdf. Mean and variance of J decrease with increasing values of κ. This behavior is expected, given the nature of κ, high values of this parameter being related to significant blockage of gas molecules on the geomaterial surface.

3.3 Scaling of gas flow model and identification of dominant flow mechanisms

A pure diffusion modeling approach has been shown to represent with an acceptable degree of accuracy the movement of methane in low permeability media (Lu et al., 2015). Such a model embeds all physics governing the system dynamics in a unique parameter (i.e., a diffusion coefficient D) and, under steady-state conditions, the mass flow-rate of methane can be expressed as:

$$J_d = -D\frac{\partial C}{\partial l}, \tag{11}$$

where $\partial C/\partial l$ represents the spatial gradient of methane concentration (C), i.e., the driving force of the system. Considering an isothermal system under single-phase flow and introducing the density of methane, $\rho = pM/RTZ$, Equation (11) can be written as:

$$J_d = -\frac{DM}{RTZ}\left(1 - \frac{p}{Z}\frac{dZ}{dp}\right)\frac{\partial p}{\partial l}. \tag{12}$$

We complete our set of results and discussion by noting that the model illustrated in Section 2.1 coincides with a pure diffusion model (Equation (12)) under single-phase conditions, as we illustrate in the following.

Equation (1) can be written as:

$$J = -B\frac{\partial p}{\partial l}, \tag{13}$$

with $B = B_v + B_k + B_{ss}$, where

$$\begin{aligned} B_v &= w_v\zeta_{mb}\frac{r^2pM}{8\eta ZRT}(1+\alpha K_n)\left(1+\frac{4K_n}{1+K_n}\right), \\ B_k &= w_k\frac{2}{3}\zeta_{mb}r\delta^{D_f-2}\left(\frac{8ZM}{\pi RT}\right)^{1/2}\frac{p}{Z}C_g, \\ B_{ss} &= \zeta_{ms}\frac{D_sC_{sc}}{p}. \end{aligned} \tag{14}$$

Comparing Equations (12) and (13), it can be seen that the diffusion coefficient D can be decomposed according to each flow mechanism as:

$$D = D_v + D_k + D_{ss}, \tag{15}$$

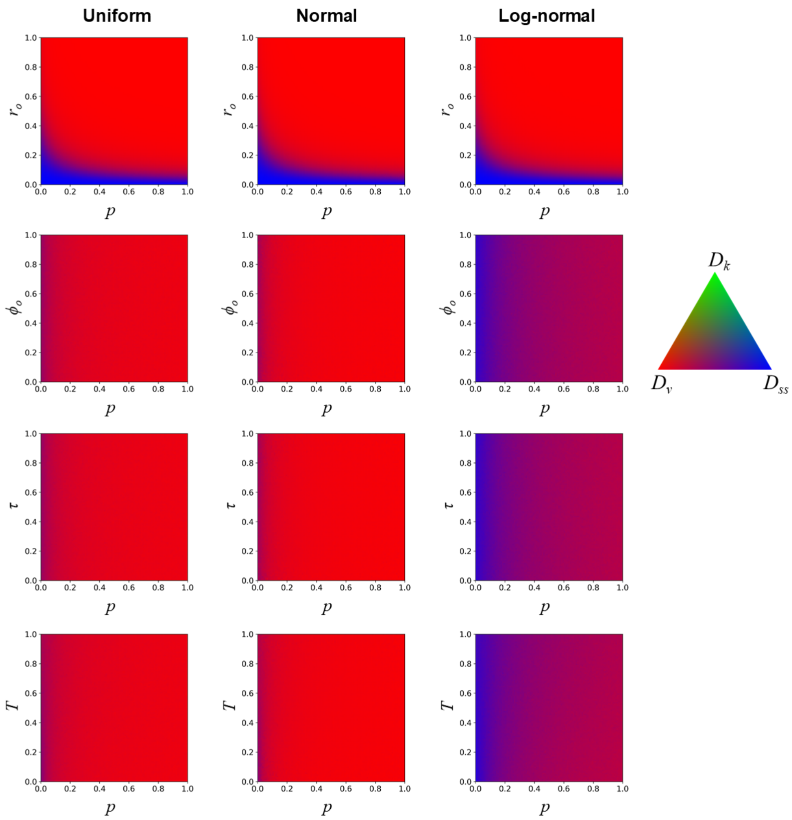

Fig. 3 Relative contribution of the effective diffusion coefficients (D_v, D_k, and D_{ss}) to the overall diffusion coefficient D rendered by Equations (15) and (16). Intervals of variation of the uncertain model parameters are rescaled within the unit interval for graphical representation purposes.

with

$$D_i = \frac{B_i \; RTZ}{M\left(1 - \frac{p}{Z}\frac{dZ}{dp}\right)}, \tag{16}$$

where $i = v, k, ss$. Note that we introduce three effective diffusion coefficients in Equation (15). These are respectively associated with the slip flow (D_v), the Knudsen diffusion (D_k), and the surface diffusion (D_{ss}) components of model (1) and are to the best of our knowledge, new for the flow model considered in this work. The variety of mechanisms included in model (1) are fully encapsulated in an overall diffusion coefficient D as illustrated in Equations (12), (15), and (16), where the contribution of each of the processes described in Section 2.1 is clearly recognizable.

Figure 3 depicts color maps quantifying the relative strength of the contribution of the three flow mechanism (slip flow in red, Knudsen diffusion in green, and surface diffusion in blue) to the overall diffusion coefficient defined by Equation (15) considering various combinations of all uncertain parameters embedded in

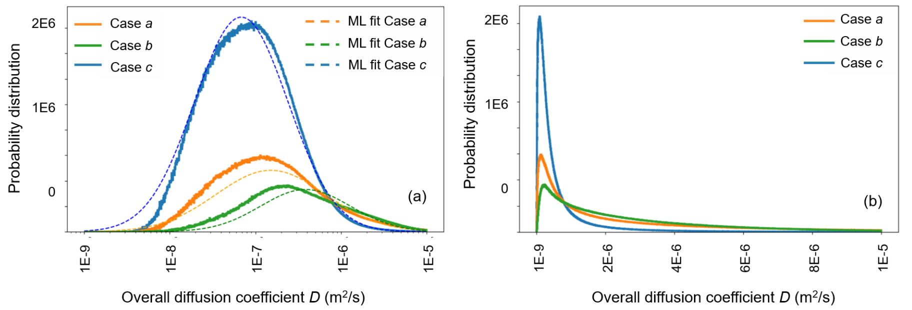

Fig. 4 Probability density functions (in logarithmic (a) and natural (b) scale) of the overall diffusion coefficient rendered by Equation (15) for model parameters characterized by: (i) uniform distributions (Case *a*), (ii) truncated normal distributions (Case *b*), and (iii) uniform distributions with the exception of r_o which is represented by a log-normal distribution (Case *c*). Dashed curves represent a ML- based fit with a log-normal model for each case

Table 5 Sample mean, variance, coefficient of variation, skewness, and kurtosis of the overall diffusion coefficient D (m^2/s) (Equation (15)) together with parameters of log-normal models (μ and σ) evaluated through ML fits against sample pdfs.

Feature	Case *a*	Case *b*	Case *c*
Mean ($\times 10^{-6}$)	3.14	2.96	0.78
Variance ($\times 10^{-12}$)	16.3	9.53	2.46
CV	1.29	1.04	2.01
Skewness	2.21	1.95	5.90
Kurtosis	9	8.1	53.54
μ	-13.53	-13.31	-14.92
σ	1.47	1.21	1.26

Equation (1) for all scenarios investigated. Each sub-plot depicts the average value of the ratio D_i/D as a function of two parameters (i.e., averaging is performed with respect to uncertain parameters with the exception of the two varying along the (normalized) axes of the subplots), selected amongst those which were classified as most influential to the system (see Sections 3.1 and 3.2).

Our results indicate that the dominant flow mechanism in defining the overall diffusion coefficient (and consequently the methane flow) is slip flow (in red in Figure 3) in all of the analyzed cases. An exception is observed for small values of the reference pore radius and/or small pore pressure, where surface diffusion is dominant. The contribution of Knudsen diffusion mechanism is always negligible. This suggests that it is possible to simplify Equation (1) by neglecting the Knudsen diffusion mechanism in the evaluation of methane flow.

Further simplifications of the methane flux model illustrated in Section 2.1 can be considered when the dominance of a given flow mechanism can be clearly established. For example, Figure 3 suggests that the identification of the dominant flow mechanism is affected by the pdf of the uncertain model parameters. If r_o is represented by a Gaussian (or uniform) pdf, J is mainly dominated by slip flow or surface diffusion with a sharp transition zone between these two mechanisms. Otherwise, when r_o is represented by a log-normal pdf both mechanisms (i.e., slip flow and surface diffusion) may play an important role in the estimation of methane migration independent of the value of the model parameters.

Finally, we evaluate the pdf of the overall diffusion coefficient (D) by making use of Equations (15) and (16) for all scenarios analyzed. Sample pdfs as well as corresponding Maximum Likelihood (ML) fits of log-normal distributions are depicted in Figure 4 in logarithmic and natural scales. Positive skewness and large kurtosis are evident for all cases, these being larger for Case c, as illustrated in Section 3.2. These results reinforce the observation of higher frequencies of low J values in Case c with respect to the other settings investigated. Sample statistical moments (mean, variance, coefficient of variation, skewness, and kurtosis) of the pdf of D are listed in Table 5 together with the parameters of the ML-based log-normal models. The overall diffusion coefficient can vary across about four orders of magnitude (i.e., between 10^{-9} and 10^{-5} m^2/s). As expected, the largest variance of D is associated with Case a, where all parameters of model (1) are characterized by uniform pdfs. Otherwise, the largest coefficient of variation of D is associated with Case c. Finally, we remark that the results embedded in Figure 4 can be of practical assistance, as they allow for fast evaluations of the probability that methane flow in low permeability media exceeds a given threshold value.

4 Conclusions

We perform a rigorous Global Sensitivity Analysis (GSA) to assess the impact of uncertain model parameters on the evaluation of methane flow (J) in low permeability media, such as caprocks. We study three cases that consider differing characterizations of the probability density function (pdf) describing model uncertain parameters to assess the impact of this choice on the results of the analysis. Such cases are: (i) all model parameters represented through uniform pdfs, (ii) all model parameters represented through (truncated) Gaussian pdfs, and (iii) reference pore radius characterized by a (truncated) log-normal pdf while all remaining parameters are associated with uniform pdfs.

Our work leads to the following main conclusions:

1. The uncertainty of methane flow is governed by uncertainty in the reference pore radius, followed (in decreasing order of importance) by reference porosity, pore pressure, tortuosity, temperature, and (to a lesser extent) blockage migration ratio of adsorbed molecules. The remaining parameters of the investigated model (Section 2.1) being practically uninfluential. This result can assist future efforts to allocate resources during experimental activities aimed at characterizing methane flow in caprocks.
2. The gas flow model introduced by Wu et al. (2016) (Section 2.1) can be related to a simple pure diffusion model by introducing an overall diffusion coefficient (D). The latter represented by the contribution of three effective diffusion coefficients, each associated with a well-defined flow mechanism. The ensuing mathematical structure of D allows distinguishing the relative contribution of all flow mechanisms to the overall methane flow. The relationship we derive also enables one to estimate the pdf of D when the model parameters are uncertain. The latter is a useful tool which can assist the probabilistic evaluation of J even in the absence of the detailed amount of information which is typically required to characterize the full methane flow model.
3. The shape of the pdf employed to characterize uncertain model parameters affects the results of our GSA. Additionally, it has a marked effect in the defi-

nition of the dominating transport mechanisms of the model. With reference to the model parameter variability considered in this study, as evaluated on the basis of available information, our results suggest that the dominant transport mechanism is slip flow. Surface diffusion plays also an important role, especially for low values of reference pore radius and pore pressure, while Knudsen diffusion is negligible in all of the test cases analyzed.

Appendix: Additional mathematical details related to the description of the gas flow model introduced in Section 2.1

The correction factor ζ_{ms} is given by

$$\zeta_{ms} = \frac{\phi}{\tau}\left(1 - \frac{r_{ad}}{r}\right)^2 \left[\left(1 - \frac{r_{ad}}{r}\right)^{-2} - 1\right], \tag{17}$$

with

$$r_{ad} = r - d_m\theta, \tag{18}$$

$$r = r_o\left(\frac{p_c - p}{p_o}\right)^{-t}, \tag{19}$$

$$\phi = \phi_o\left(\frac{p_c - p}{p_o}\right)^{-q}, \tag{20}$$

where r_{ad} is thickness of the adsorbed gas layer, d_m is gas molecule diameter, p_c is overburden pressure, p_o is atmospheric pressure, and θ is evaluated through a Langmuir equilibrium isotherm as:

$$\theta = \frac{p/Z}{p_L + p/Z}, \tag{21}$$

where p_L is a Langmuir pressure evaluated with

$$p_L = p_{L_o}\exp\left(-\frac{\Delta H}{RT}\right). \tag{22}$$

The correction factor ζ_{mb} is expressed as

$$\zeta_{mb} = \frac{\phi}{\tau}\left(1 - \frac{r_{ad}}{r}\right)^2. \tag{23}$$

The value of α (in Eq. (7)) is evaluated through

$$\alpha = \alpha_0\frac{2}{\pi}\tan^{-1}\left(\alpha_1 K_n^{\beta}\right), \tag{24}$$

where uncertain parameters α_0, α_1, and β allow to represent the variation of α as a function of Knudsen number (K_n). Here, α_0 represents the maximum value of α for large values of K_n, α_1 governs the values of α for small values of K_n, and β defines the slope of the relationship between K_n and α for low values of K_n.

The surface diffusion coefficient (D_s) is given by

$$D_s = D_s^0 \frac{(1-\theta) + \frac{\kappa}{2}\theta(2-\theta) + H(1-\kappa)(1-\kappa)\frac{\kappa}{2}\theta^2}{\left(1-\theta+\frac{\kappa}{2}\theta\right)^2}, \tag{25}$$

with

$$D_s^0 = 8.29 \times 10^{-7} \exp\left(-\frac{\Delta H^{0.8}}{RT}\right), \tag{26}$$

$$H(1-\kappa) = \begin{cases} 0, & \text{if } \kappa \geq 1 \\ 1, & 0 \leq \kappa \leq 1 \end{cases}. \tag{27}$$

The adsorbed concentration (C_{sc}) is given by

$$C_{sc} = \frac{4\theta M}{\pi d_m^3 N_A}, \tag{28}$$

where N_A is the Avogadro Constant ($6.02{\times}10^{-23}$/mol).

List of Symbols and Nomenclature

Symbol	Refers to	Units	Evaluated
C_g	Gas compressibility	1/MPa	MiniREFPROP
C_{sc}	Adsorbed concentration	kg/m^3	Equation 28
d_m	Gas molecule diameter	nm	0.38
$\partial p/\partial l$	Gradient of gas pore pressure	MPa/m	0.1
D	Overall diffusion coefficient	m^2/s	Equation 15
D_s	Surface diffusion coefficient	m^2/s	Equation 25
D_k	Knudsen effective diffusion coefficient	m^2/s	Equation 16
D_{ss}	Surface effective diffusion coefficient	m^2/s	Equation 16
D_v	Slip flow effective diffusion coefficient	m^2/s	Equation 16
J	Mass flux of gas per unit of area	kg/(m^{2}s)	Equation 1
J_k	Knudsen diffusion	kg/(m^{2}s)	Equation 8
J_s	Surface diffusion	kg/(m^{2}s)	Equation 2
J_v	Slip flow	kg/(m^{2}s)	Equation 7
Kn	Knudsen number	-	Equation 5
M	Gas molar mass	kg/mol	1.6×10^{-2}
p_L	Langmuir pressure	MPa	Equation 22
p_o	Atmospheric pressure	MPa	0.1
r	Pore size	nm	Equation 19
R	Universal gas constant	J/(mol K)	8,3144
r_{ad}	Thickness of adsorbed gas layer	nm	Equation 18
w_k	Knudsen diffusion flux weight factor	-	Equation 4
w_v	Slip mass flux weight factor	-	Equation 3
Z	Gas deviation factor	-	MiniREFPROP
α	Rarified effect coefficient for gas	-	Equation 24
ζ_{ms}	Correction factor of surface diffusion	-	Equation 17
ζ_{mb}	Correction factor bulk flow	-	Equation 23

η	Gas viscosity	Pa s	MiniREFPROP
θ	Gas coverage of the geomaterial	-	Equation 21
λ	Mean free path of gas molecules	m	Equation 6
ϕ	Porosity	-	Equation 20

Declarations

Funding. The authors acknowledge financial support from Geolog srl.
Competing interests. Not applicable
Availability of data and material All data used in the paper will be retained by the authors for at least 5 years after publication and will be available to the readers upon request.
Code availability. Codes used in this paper are available in the following github repository `https://github.com/rlsandovalp/Sensitivity_Analysis`

References

Bianchi Janetti E, Guadagnini L, Riva M, Guadagnini A (2019) Global sensitivity analyses of multiple conceptual models with uncertain parameters driving groundwater flow in a regional-scale sedimentary aquifer. Journal of Hydrology 574(September 2018):544–556, DOI 10.1016/j.jhydrol.2019.04.035

la Cecilia D, Porta GM, Tang FH, Riva M, Maggi F (2020) Probabilistic indicators for soil and groundwater contamination risk assessment. Ecological Indicators 115:106,424, DOI 10.1016/j.ecolind.2020.106424

Ceresa L, Guadagnini A, Porta GM, Riva M (2021) Formulation and probabilistic assessment of reversible biodegradation pathway of Diclofenac in groundwater. Water Research 204:117,466, DOI 10.1016/J.WATRES.2021.117466

Chiquet P, Daridon JL, Broseta D, Thibeau S (2007) CO2/water interfacial tensions under pressure and temperature conditions of CO2 geological storage. Energy Conversion and Management 48(3):736–744, DOI 10.1016/J.ENCONMAN.2006.09.011

Ciriello V, Guadagnini A, Di Federico V, Edery Y, Berkowitz B (2013) Comparative analysis of formulations for conservative transport in porous media through sensitivity-based parameter calibration. Water Resources Research 49(9):5206–5220, DOI 10.1002/wrcr.20395

Civan F (2010) Effective correlation of apparent gas permeability in tight porous media. Transport in Porous Media 82(2):375–384, DOI 10.1007/s11242-009-9432-z

Colombo I, Porta GM, Ruffo P, Guadagnini A (2017) Uncertainty quantification of overpressure buildup through inverse modeling of compaction processes in sedimentary basins. Hydrogeology Journal 25(2):385–403, DOI 10.1007/s10040-016-1493-9

Coppens MO (1999) The effect of fractal surface roughness on diffusion and reaction in porous catalysts – from fundamentals to practical applications. Catalysis Today 53(2):225–243, DOI 10.1016/S0920-5861(99)00118-2

Coppens MO, Dammers AJ (2006) Effects of heterogeneity on diffusion in nanopores—From inorganic materials to protein crystals and ion channels. Fluid Phase Equilibria 241(1-2):308–316, DOI 10.1016/J.FLUID.2005.12.039

Darabi H, Ettehad A, Javadpour F, Sepehrnoori K (2012) Gas flow in ultra-tight shale strata. Journal of Fluid Mechanics 710:641–658, DOI 10.1017/jfm.2012.424

Dell'Oca A, Riva M, Guadagnini A (2017) Moment-based metrics for global sensitivity analysis of hydrological systems. Hydrology and Earth System Sciences 21(12):6219–6234, DOI 10.5194/hess-21-6219-2017

Dell'Oca A, Riva M, Guadagnini A (2020) Global Sensitivity Analysis for Multiple Interpretive Models With Uncertain Parameters. Water Resources Research 56(2):1–20, DOI 10.1029/2019WR025754

Dembicki-Jr H (2017) Petroleum Geochemistry for Exploration and Production. Candice Janco, DOI 10.1016/j.jhsb.2006.10.005

Dong JJ, Hsu JY, Wu WJ, Shimamoto T, Hung JH, Yeh EC, Wu YH, Sone H (2010) Stress-dependence of the permeability and porosity of sandstone and shale from TCDP Hole-A. International Journal of Rock Mechanics and Mining Sciences 47(7):1141–1157, DOI 10.1016/J.IJRMMS.2010.06.019

Hughes JD (2013) Energy: A reality check on the shale revolution. Nature 494(7437):307–308, DOI 10.1038/494307a

Javadpour F, Singh H, Rabbani A, Babaei M, Enayati S (2021) Gas Flow Models of Shale: A Review. Energy and Fuels 35(4):2999–3010, DOI 10.1021/acs.energyfuels.0c04381

Karniadakis G, Beskok A, Aluru N (2005) Microflows and Nanoflows. (Springer Science+Business Media, Inc, DOI 10.1103/PhysRevE.67.041106

Koks EE, Bočkarjova M, de Moel H, Aerts JC (2015) Integrated direct and indirect flood risk modeling: Development and sensitivity analysis. Risk Analysis 35(5):882–900, DOI 10.1111/risa.12300

Laloy E, Rogiers B, Vrugt JA, Mallants D, Jacques D (2013) Efficient posterior exploration of a high-dimensional groundwater model from two-stage Markov chain Monte Carlo simulation and polynomial chaos expansion. Water Resources Research 49(5):2664–2682, DOI 10.1002/wrcr.20226

Lemmon EW, Bell I, Huber ML, McLinden MO (2018) NIST Standard Reference Database 23: Reference Fluid Thermodynamic and Transport Properties-REFPROP, Version 10.0, National Institute of Standards and Technology. DOI https://doi.org/10.18434/T4/1502528

Li Z, Dong M, Li S, Huang S (2006) CO2 sequestration in depleted oil and gas reservoirs—caprock characterization and storage capacity. Energy Conversion and Management 47(11-12):1372–1382, DOI 10.1016/J.ENCONMAN.2005.08.023

Liu J, Wang JG, Gao F, Ju Y, Zhang X, Zhang LC (2016) Flow Consistency Between Non-Darcy Flow in Fracture Network and Nonlinear Diffusion in Matrix to Gas Production Rate in Fractured Shale Gas Reservoirs. Transport in Porous Media 111(1):97–121, DOI 10.1007/s11242-015-0583-9

Lu J, Larson TE, Smyth RC (2015) Carbon isotope effects of methane transport through Anahuac Shale - A core gas study. Journal of Geochemical Exploration 148:138–149, DOI 10.1016/j.gexplo.2014.09.005

Maina FZ, Siirila-Woodburn ER (2020) The Role of Subsurface Flow on Evapotranspiration: A Global Sensitivity Analysis. Water Resources Research 56(7):1–20, DOI 10.1029/2019WR026612

Maina FZ, Guadagnini A, Riva M (2021) Impact of multiple uncertainties on gravimetric variations across randomly heterogeneous aquifers during pumping. Advances in Water Resources 154:103,978, DOI 10.1016/J.ADVWATRES.2021.103978

Mehmani A, Prodanović M, Javadpour F (2013) Multiscale, Multiphysics Network Modeling of Shale Matrix Gas Flows. Transport in Porous Media 99(2):377–390, DOI 10.1007/s11242-013-0191-5

Mohd Amin S, Weiss DJ, Blunt MJ (2014) Reactive transport modelling of geologic CO2 sequestration in saline aquifers: The influence of pure CO2 and of mixtures of CO2 with CH4 on the sealing capacity of cap rock at 37°C and 100bar. Chemical Geology 367:39–50, DOI 10.1016/J.CHEMGEO.2014.01.002

Naraghi ME, Javadpour F, Ko LT (2018) An Object-Based Shale Permeability Model: Non-Darcy Gas Flow, Sorption, and Surface Diffusion Effects. Transport in Porous Media 125(1):23–39, DOI 10.1007/s11242-017-0992-z

Pan Z, Connell LD, Camilleri M, Connelly L (2010) Effects of matrix moisture on gas diffusion and flow in coal. Fuel 89(11):3207–3217, DOI 10.1016/j.fuel.2010.05.038

Rani S, Prusty BK, Pal SK (2018) Adsorption kinetics and diffusion modeling of CH4 and CO2 in Indian shales. Fuel 216(November 2017):61–70, DOI 10.1016/j.fuel.2017.11.124

Saltelli A, Sobol' IM (1995) Sensitivity analysis for nonlinear mathematical models: numerical experience (in Russian). Mathematical models and computer experiment 7(11):16–28

Saltelli A, Annoni P, Azzini I, Campolongo F, Ratto M, Tarantola S (2010) Variance based sensitivity analysis of model output. Design and estimator for the total sensitivity index. Computer Physics Communications 181(2):259–270, DOI 10.1016/j.cpc.2009.09.018

Schloemer S, Krooss BM (2004) Molecular transport of methane, ethane and nitrogen and the influence of diffusion on the chemical and isotopic composition of natural gas accumulations. Geofluids 4(1):81–108, DOI 10.1111/j.1468-8123.2004.00076.x

Schlömer S, Krooss BM (1997) Experimental characterisation of the hydrocarbon sealing efficiency of cap rocks. Marine and Petroleum Geology 14(5):565–580, DOI 10.1016/S0264-8172(97)00022-6

Setzmann U, Wagner W (1991) A New Equation of State and Tables of Thermodynamic Properties for Methane Covering the Range from the Melting Line to 625 K at Pressures up to 100 MPa. Journal of Physical and Chemical Reference Data 20(6):1061–1155, DOI 10.1063/1.555898

Singh H, Myong RS (2018) Critical Review of Fluid Flow Physics at Micro- to Nano-scale Porous Media Applications in the Energy Sector. Advances in Materials Science and Engineering 2018, DOI 10.1155/2018/9565240

Sochala P, Le Maître OP (2013) Polynomial Chaos expansion for subsurface flows with uncertain soil parameters. Advances in Water Resources 62:139–154, DOI 10.1016/j.advwatres.2013.10.003

Song W, Yao J, Li Y, Sun H, Zhang L, Yang Y, Zhao J, Sui H (2016) Apparent gas permeability in an organic-rich shale reservoir. Fuel 181:973–984, DOI 10.1016/j.fuel.2016.05.011

Sun Z, Li X, Shi J, Zhang T, Sun F (2017) Apparent permeability model for real gas transport through shale gas reservoirs considering water distribution characteristic. International Journal of Heat and Mass Transfer 115:1008–1019, DOI 10.1016/j.ijheatmasstransfer.2017.07.123

Tan Y, Pan Z, Liu J, Kang J, Zhou F, Connell LD, Yang Y (2018) Experimental study of impact of anisotropy and heterogeneity on gas flow in coal. Part I: Diffusion and adsorption. Fuel 232(15):444–453, DOI 10.1016/j.fuel.2018.05.173

US Energy Information Administration (2015) World Shale Resource Assessments. URL `https://www.eia.gov/analysis/studies/worldshalegas/`

Wang T, Tian S, Li G, Zhang P (2019) Analytical Model for Real Gas Transport in Shale Reservoirs with Surface Diffusion of Adsorbed Gas. Industrial and Engineering Chemistry Research 58(51):23,481–23,489, DOI 10.1021/acs.iecr.9b05630

Wu K, Chen Z, Li X (2015a) Real gas transport through nanopores of varying cross-section type and shape in shale gas reservoirs. Chemical Engineering Journal 281:813–825, DOI 10.1016/j.cej.2015.07.012

Wu K, Li X, Wang C, Yu W, Chen Z (2015b) Model for surface diffusion of adsorbed gas in nanopores of shale gas reservoirs. Industrial and Engineering Chemistry Research 54(12):3225–3236, DOI 10.1021/ie504030v

Wu K, Chen Z, Li X, Guo C, Wei M (2016) A model for multiple transport mechanisms through nanopores of shale gas reservoirs with real gas effect-adsorption-mechanic coupling. International Journal of Heat and Mass Transfer 93:408–426, DOI 10.1016/j.ijheatmasstransfer.2015.10.003

Wu K, Chen Z, Li X, Xu J, Li J, Wang K, Wang H, Wang S, Dong X (2017) Flow behavior of gas confined in nanoporous shale at high pressure: Real gas effect. Fuel 205:173–183, DOI 10.1016/j.fuel.2017.05.055

Xiao S, Praditia T, Oladyshkin S, Nowak W (2021) Global sensitivity analysis of a CaO/Ca(OH)2 thermochemical energy storage model for parametric effect analysis. Applied Energy 285(December 2020):116,456, DOI 10.1016/j.apenergy.2021.116456

Yuan W, Pan Z, Li X, Yang Y, Zhao C, Connell LD, Li S, He J (2014) Experimental study and modelling of methane adsorption and diffusion in shale. Fuel 117(PART A):509–519, DOI 10.1016/j.fuel.2013.09.046

Zhang Q, Su Y, Wang W, Lu M, Sheng G (2018) Gas transport behaviors in shale nanopores based on multiple mechanisms and macroscale modeling. International Journal of Heat and Mass Transfer 125:845–857, DOI 10.1016/j.ijheatmasstransfer.2018.04.129

Ziarani AS, Aguilera R (2012) Knudsen's Permeability Correction for Tight Porous Media. Transport in Porous Media 91(1):239–260, DOI 10.1007/s11242-011-9842-6